CrossMark

An Improved ERT Approach for the Investigation of Subsurface Structures

De-Bao Lu,[1] Feng Wang,[1] Xiao-Dong Chen,[1] Jian Ou,[1] and Hui Wang[1]

Abstract—The joint use of multiple geophysical data types has been proven to be a powerful tool to both improve subsurface imaging and help in the interpretation process. The main goal of this paper is to develop a multi-geophysical approach for subsurface experimental investigations in which seismic data are used to improve electrical resistivity tomography quality. The basic philosophy of the method is that seismic travel time data will be used to construct the prior model for the resistivity inversion. Synthetic data were employed to demonstrate the improvements enabled by the use of this strategy. Afterwards, the scheme was applied successfully on field data from northwestern China. The outcomes reveal that the multi-geophysical approach improves the interpretation of the subsurface over a single source.

Key words: ERT, SRT, prior model, velocity model, inversion.

1. Introduction

Electrical resistivity tomography (ERT) has proven to be a powerful tool in the exploration of underground structures in many fields (Page 1968; White et al. 2001; Bauman 2005; Wilson et al. 2006; Chambers et al. 2006; Legault et al. 2008). This method is particularly useful for subsurface image construction. However, with the increasing need for improved characterization of near-surface regions, a single source of geophysical data is insufficient to provide results of necessary accuracy. A great deal of work has been done on combining several geophysical data sources such as ERT, ground-penetrating radar, and seismic reflection tomography (SRT) data to obtain better characterization of subsurface features (Cardarelli et al. 2010; Beauvais et al. 2004).

The imaging of geologic formations is generally of great importance in understanding faults and fractured zones using seismic methods (Haeni 1986; Mela and Louie 2001; Jarvis and Knight 2002). Sumanovac and Weisser (2001) and Balia et al. (2003) showed that the combination of electrical and seismic tomographies was the most appropriate methodology to image fresh and saline water subsurface zones. There are two ways to combine electrical and seismic data. The first is not truly a combination but rather a joint use of the two data sources. Leucci et al. (2007) used 3-D seismic data to aid in the interpretation of electrical resistivity data. Compared with results from each method applied, the approach showed potential advantages. However, in this method, the experimental data are always interpreted using separate inversion schemes for each method, which can lead to results that do not always agree. The second method uses multidimensional joint inversion, which is helpful in interpreting complicated near-surface structures. Gallardo and Meju (2004) presented a 2-D joint structural inversion approach using a cross-gradients function. Based on this work, Hamdan and Vafidis (2013) developed joint inversion strategies to provide improved resistivity and seismic velocity images to delineate saline water zones in karstic geological formations. Although joint inversion has proven useful in the interpretation of field data, certain drawbacks exist, including the use of complicated algorithms and an uncertain damping factor. In particular, this method has limitations with respect to improving the quality of ERT. Therefore, a rapid and efficient method that can provide higher quality imaging and the ability to combine ERT data with SRT data is needed.

In this paper, a program is developed using C++ on a Linux platform to combine ERT and SRT data to improve ERT data quality. The program is designed

[1] Institute of Hydraulic and Environmental Engineering, Zhejiang University of Water Resources and Electric Power, Hangzhou 310018, China. E-mail: luderbor@gmail.com

for both 2-D and 3-D cases. However, in this study, all measurements are dependent on a 2-D profile, and only a 2-D case is discussed. This study differs from previous studies in the sense that, here, the SRT data are deployed as a prior model for the ERT inversion process. To demonstrate the reasonableness and reliability of the method, synthetic data, including one block and two blocks, were tested with a different prior model. Based on the results, the method is applied to the case of Beishan, Gansu Province, China.

2. Methodology

2.1. The Basic Idea of Combining Two Geophysical Data

Geophysics data inversion is used to reproduce measured data with calculated model parameters. A better prior model involved by inversion will not only provide more accurate result but also save a considerable amount of calculation time as it converges during the calculation procedure (Tarantola 1987). The basic idea underlying our approach is that seismic travel time data will be used to construct the prior model for the resistivity inversion. The scheme is outlined in Fig. 1 and completely depends on the inversion calculation of the seismic and resistivity data. The integrated method is actually a sequential approach to joint resistivity and seismic inversion. Seismic data inversion result will be used as constraint condition input for ERT inversion after transformation. As we know, the perturbation vector for the model parameter during the ERT inversion can be given by (Tarantola and Valette 1982):

$$(S_k^T R_{dd}^{-1} S_k + R_{mm}^{-1})\Delta\rho_k = S_k^T R_{dd}^{-1}(d - G(\rho_k)) \\ + R_{mm}^{-1}(\rho_0 - \rho_k) \qquad (1)$$

where S is the sensitivity matrix; d is the observed data vector; ρ is the model parameter vector; G is the forward modelling operator; R_{dd} and R_{mm} are the covariance matrices for the data and model parameter, respectively; ρ_0 is the prior parameter vector (prior model); $\Delta\rho_k$ is the kth perturbation vector for inversion iteration. To solve this equation, an

algorithm that can provide a suitable initial model resistivity (ρ_0) is very important (Tarantola 1987). Some researchers try to use an averaging model (Dahlin et al. 2002) to accelerate the convergence when solving the equations. In our research, the conversed model from seismic data is applied to solve the problem instead of averaging model.

The key element of the proposed approach is the identification of the intimate relation between resistivity and seismic data, which determine the electrical and acoustic responses of subsurface structures, respectively. To convert seismic data inversion results to the resistivity model, the equation proposed by Meju et al. (2003) is adopted, which can be reasonably used as the prior model for electrical resistivity tomography (ERT) inversion. This equation provides the link between the electrical resistivity and the seismic velocity via their common thread, in which resistivity and velocity are both functions of porosity. The velocity model can be then converted to a resistivity model via the following equation:

$$Log_{10}\rho = mLog_{10}V_p + c \qquad (2)$$

where ρ is the resistivity in $\Omega \cdot m$ and V_p is the velocity of the P-wave in m/s. However, Eq. (2) is a completely empirical function obtained from inversion calculation of selected natural laboratory data. Thus, constants m and c have no physical relevance and are totally defined by the subsurface materials as $m = 3.88$ and $c = -11$ for consolidated rocks (>3 m deep) and $m = -3.88$ and $c = 13$ for unconsolidated soil or drift deposits. After several model tests, the function has proven to be reliable when converting the two different data types in our research. Thus, the converted resistivity model is adopted as the prior model for ERT inversion program.

Before this can be accomplished, it is necessary to solve the forward problem. Several techniques, including numerical methods, have been proposed to study the resistivity and seismic forward problems, which are described in following sections. To ensure that the two types of data are visible in the same scale, the same mesh was created for the finite element resistivity forward problem and is subsequently used by the ray tracing algorithm.
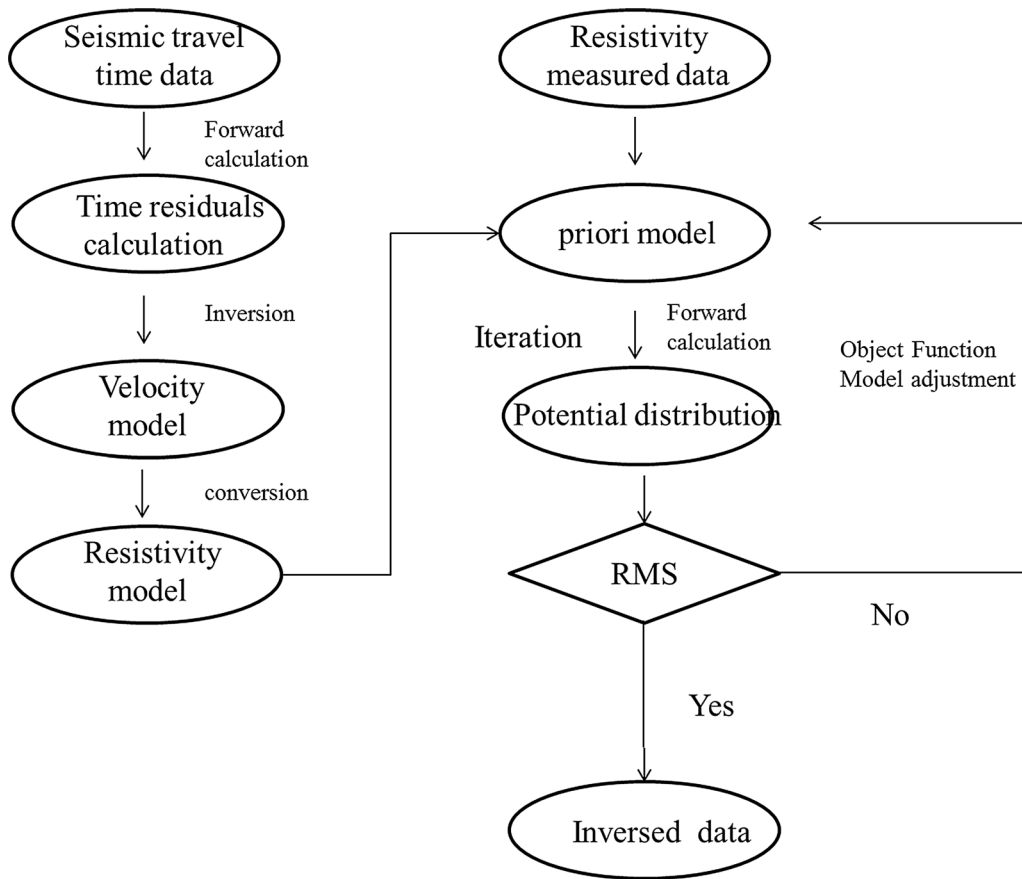
Figure 1
Process flows for multiple geophysical approach

2.2. Inversion Scheme for SRT and ERT

Vidale's (1988) forward method that calculates the first-arrival travel times on a uniform grid using a finite-differencing method is used as the original code in our research. Ray paths are obtained by following the steepest gradient of the time field from a source to the receiver (Vidale 1988). The propagation of the 2-D wavefronts is guided by the Eikonal equation for ray tracing

$$\left(\frac{\partial t}{\partial x}\right)^2 + \left(\frac{\partial t}{\partial z}\right)^2 = s(x,z)^2 \qquad (3)$$

where x and z are coordinate axes and s is the slowness. The two differential terms in Eq. (3) are approximated using a finite-difference method:

$$\frac{\partial t}{\partial x} = \frac{1}{2h}(t_0 + t_2 - t_1 - t_3) \qquad (4a)$$

and

$$\frac{\partial t}{\partial z} = \frac{1}{2h}(t_0 + t_1 - t_2 - t_3) \qquad (4b)$$

Substituting Eqs. (4a) and (4b) into Eq. (3), we obtain the following:

$$t_0 = t_3 + \sqrt{2(hs)^2 - (t_2 - t_1)^2} \qquad (5)$$

where t_n is the travel time at the nth node, h is the grid spacing, and s is the slowness (inverse velocity) of the grid cell. The travel time at the corner of the 2-D operator is calculated by the known time nodes using Eq. (5). In this way, the travel time for each node is

calculated iteratively. However, Vidale's method is invalid for large velocity gradients (Zelt and Barton 1998). In this case, the algorithm is modified according to the method presented by Hole and Zelt (1995). The algorithm is updated by a 1-D operator:

$$t_0 = t_1 + \mathrm{hs} \qquad (6)$$

which represents a head wave that propagates along the boundary between the two media at the velocity of the faster medium. Moreover, a reverse propagation using position exchanging from the source points and receiver points is employed to recalculate the travel time. Travel times from the new calculations only replace the previously computed times if the new times are smaller. Then, the iterative back-projection method described by Hole (1992) is used to conduct the inversion calculation. Zelt and Barton (1998) tested this method with real and synthetic data and proved its effectiveness and reliability. For the ERT forward and inversion problem, we implemented the technique of progressive finite element and patch method, respectively, of Lu et al. (2014).

3. Application to Synthetic Data

We test our implemented seismic and electrical resistivity tomography (ERT) inversion code using a one-block model and a two-block model, which are all relevant to the situation in Beishan, China. However, the scale and shape of the models were optimized in terms of the requirement of research.

For all synthetic models, we compared the results from the pole–pole array, which provides the better lateral resolution, with the Wenner array, which is more suitable for resolving resistivity changes with depth.

3.1. Model with One Low-Resistivity Block

The model consists of a low-resistivity (10 Ωm) block surrounded by a high-resistivity (100 Ωm) block. The P-wave velocities for the two blocks are 1000 and 2000 m/s, respectively. The size of the model (Fig. 2) is 200 × 100 m where a 20 × 20 m low-resistivity block is buried at a depth of 20 m. Synthetic apparent resistivity data are generated using a FEM as described above for the pole–pole array and Wenner array. In addition, 41 electrodes spaced at 5 m are used. Vidale's method generates first arrivals for 20 geophones that are located every 5 m and seismic sources every 50 m along the profile. The calculated travel time data are inverted to the velocity model by adding 10 % random noise using Hole's (1992) method, which is very close to observed data. According to Eq. (2), the velocity model is converted to a resistivity model, which is adopted as a prior model in the ERT scheme (Fig. 3). Additionally, the average prior model is used as a parallel parameter for comparison with the results from the converted prior model. Random noise with a normal distribution and a standard deviation of 10 % is added to the synthetic resistivity data for the ERT inversion step.
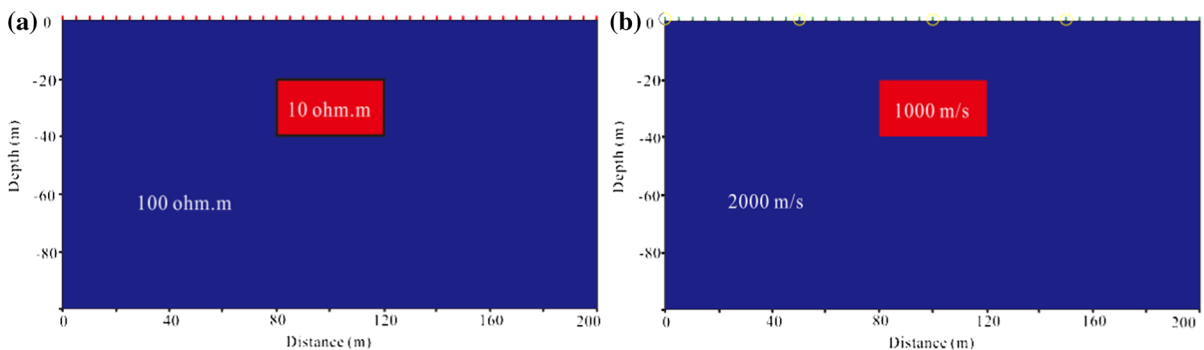

Figure 2
Synthetic model with a one-block **a** resistivity model, where the *red points* denote the position of the electrodes; and **b** a seismic velocity model, where the *green points* and *yellow circle* denote the seismic receiver and source position, respectively
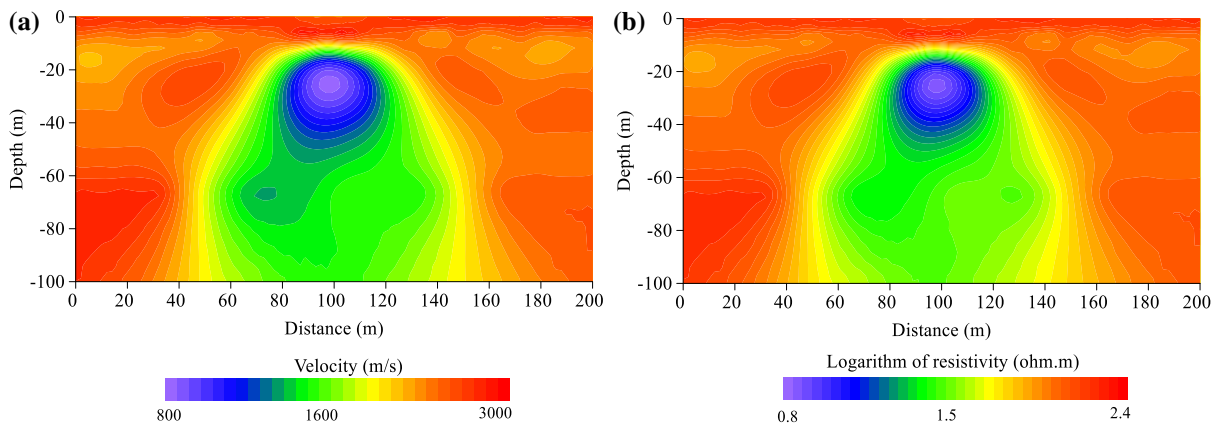
Figure 3
The calculated velocity results (**a**) and converted resistivity results (**b**) for one-block model
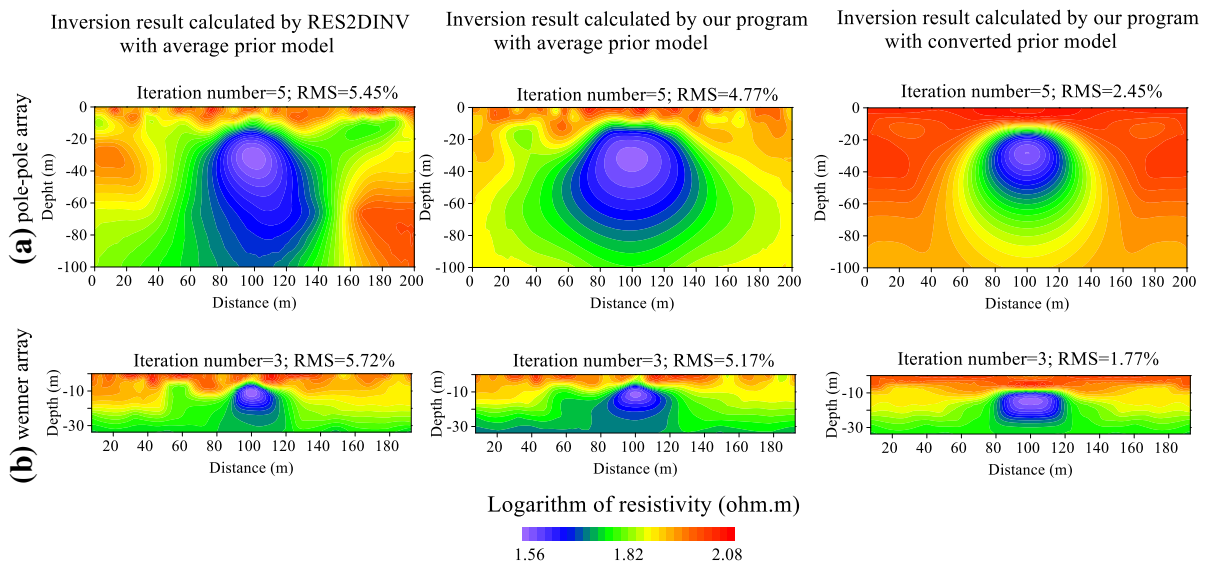

Figure 4
Inversion results calculated by different methods using different arrays for the one-block model

Figure 4 shows the outcome of the inversion calculated using RES2Dinv and our method separately. The resistivity model is properly reconstructed after the fifth iteration for the pole–pole array and the third iteration for the Wenner array. The resistivity values for the aquifer, as well as the resistivity values for the surrounding limestone, are very close to the actual values. However, the RMS level of our method is less than that of RES2Dinv for both arrays. It appears that our method provides better geometrical information on the anomaly. In particular, the results
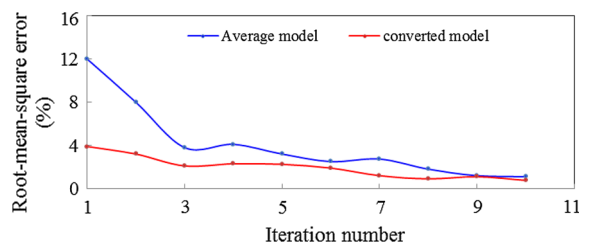

Figure 5
RMS errors of ERT inversion from different prior models using a pole–pole array
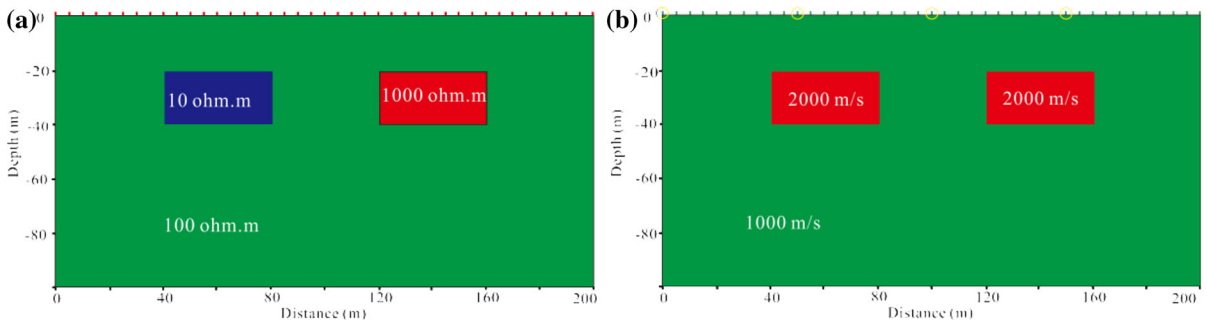
Figure 6
Synthetic model with a two-block **a** resistivity model, where the *red points* denote the position of the electrodes; and **b** a seismic velocity model, where the *green points* and *yellow circle* denote the seismic receiver and source position, respectively
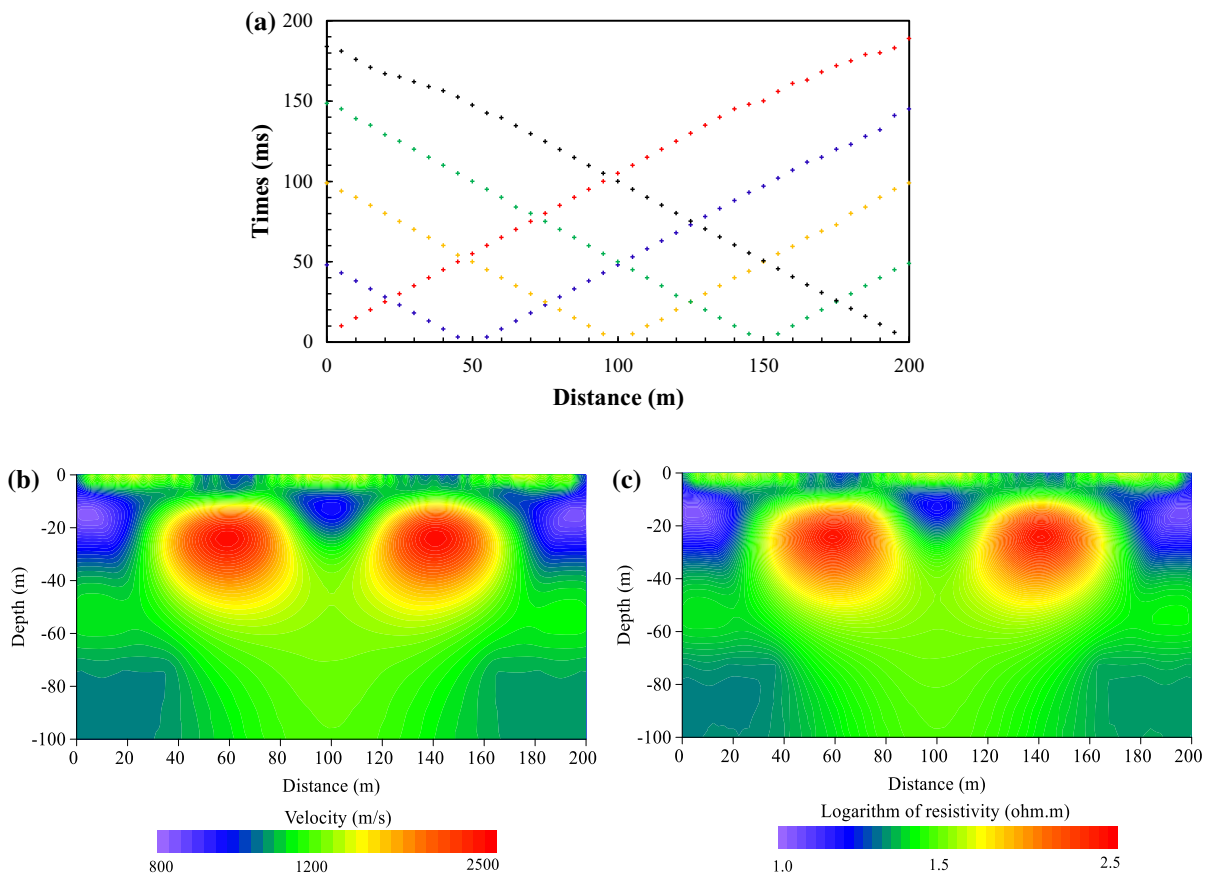

Figure 7
Computed travel time responses (**a**); calculated velocity results (**b**) and converted resistivity results (**c**) for two-block model

produced by the average prior model and converted prior models are compared. For the proposed converted prior model strategy, convergence is faster and the size and position of the region of interest are more accurate.

Figure 5 demonstrates how the RMS level is related to the iteration number. For the converted prior model, the RMS level greatly decreases after the first iteration, which demonstrates that the calculation rapidly converges during this progress.
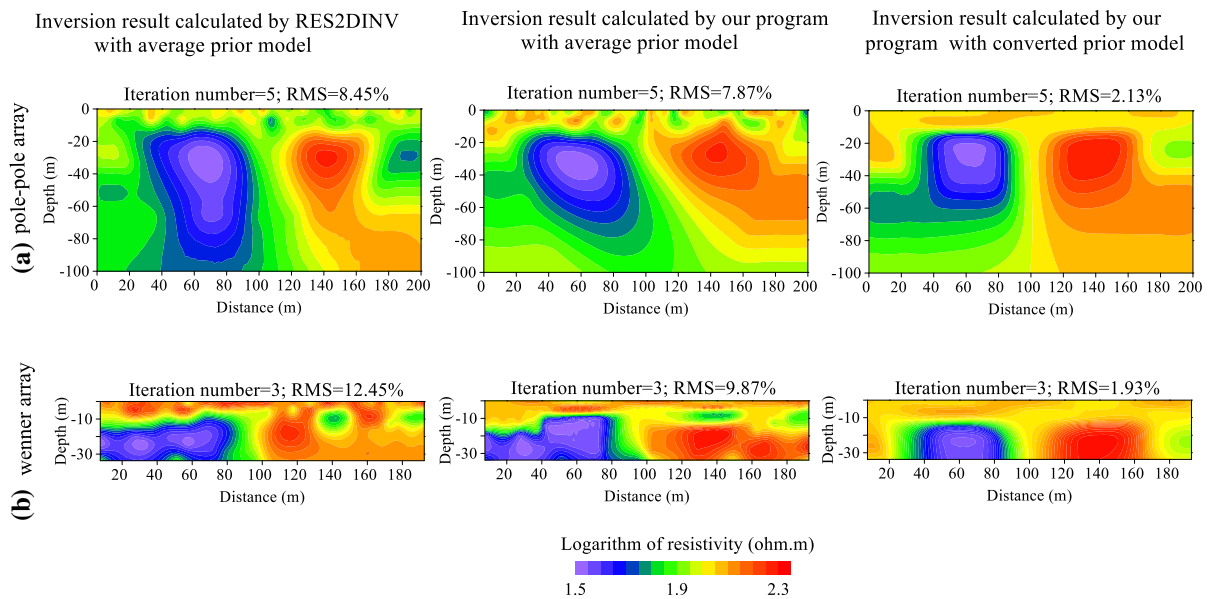
Figure 8
Inversion results calculated by different methods using different arrays for the two-block model

3.2. Two-Block Model

The 2-D model (Fig. 6) consists of two rectangular boxes with a size of 20×20 m embedded in a 200×100 m half-space with the following properties:

Half-space: $\rho = 100$ Ωm and $V_p = 1000$ m/s;
Box 1: $\rho = 10$ Ωm and $V_p = 2000$ m/s;
Box 2: $\rho = 1000$ Ωm and $V_p = 2000$ m/s.

The values of the model parameters are chosen so that one box has host–target contrasts of the same sign for both resistivity and velocity and the other box has opposite contrasts. Similar ERT and seismic travel time collection configurations are conducted on this test model. The synthetic apparent resistivity and travel time are obtained using the same method. The velocity model is produced using seismic inversion with 10 % random noise added. In addition, the average prior is applied for comparison. Figure 7 gives the computed travel time responses, calculated velocity model and the converted resistivity model which is employed as a prior model in the ERT inversion, respectively.

As shown in Fig. 8, our method provides basic information for the region of interest, whereas the information from RES2Dinv is slightly distorted
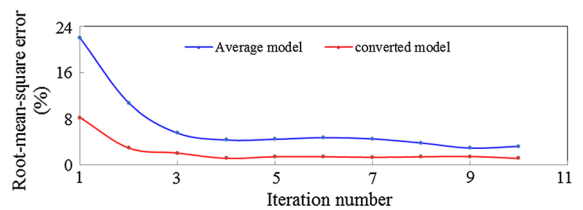

Figure 9
RMS errors of ERT inversion from different prior models using a pole–pole array

although not unacceptable. The inverted results from the two-block model are generated from the average and converted prior models. The two different prior models both recover the basic shape of the original model with a low-resistivity box located in the left part and a high-resistivity box located in the right part. However, the two-box anomalies exhibit different distribution for the two prior models. For the converted prior model, the position and size of the boxes are more precise. The low- and high-resistivity areas converge in the region where the original anomalies are set. In addition, a lower RMS level than in the average prior model appears after the fifth iteration (Fig. 9). Moreover, the error is greatly decreased after the first iteration using the converted prior model.
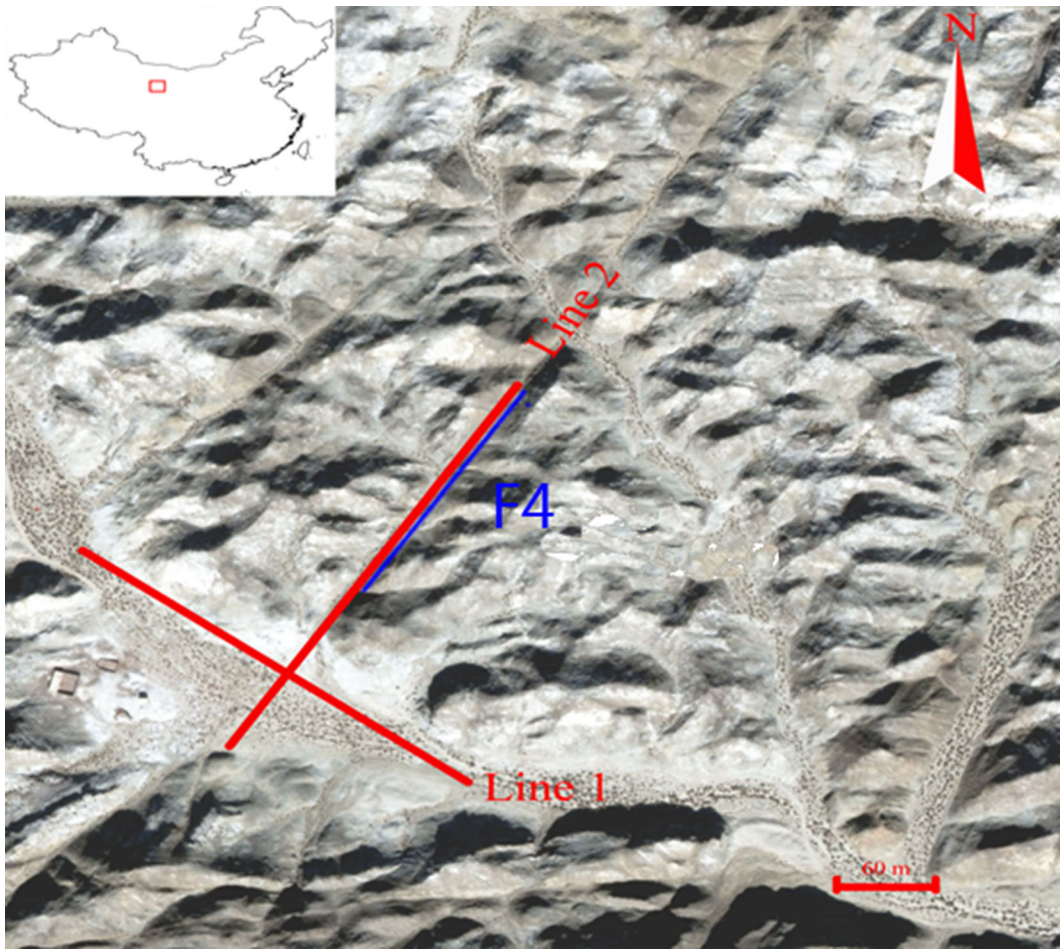
Figure 10
The location of two field survey *lines*

4. Application to Real Data

The proposed new strategy is applied for the region of Beishan, Gansu, China, which is a candidate site for high-level radioactive waste disposal. This region consists mainly of limestone and granitic rock, where Eq. (2) can be applied to approximately consolidated rock. Many fundamental studies are presently being conducted in this region. The aim of our work is to acquire rough information on the subsurface features within the area to provide a basic profile for further research. The developed scheme is applied on data from the survey line in different geophysical ways. Figure 10 shows the location of the two survey profiles where each line is 320 m in length. E60CN and SE2404EI produced by Chinese

Geopen Company are adopted to collect the apparent resistivity and travel time from Lines 1 and 2. The pole–pole array, using 64 electrodes with an electrode spacing of 5 m (315 m total length), is used for this test. The corresponding seismic tomography employed five shot points in six 12-geophone spreads and 5 m geophone spacing.

The first-arrival time is automatically picked by a computer using Coppens' (1985) method. Rectangular cells of invariant size 1×1 m are generated for ERT and SRT. With respect to different resolution of two methods, a smoothness scheme was used to keep them in same scale. To obtain a more accurate velocity model, an initial velocity model represented by the results obtained from the simple interpretation of the seismic data is
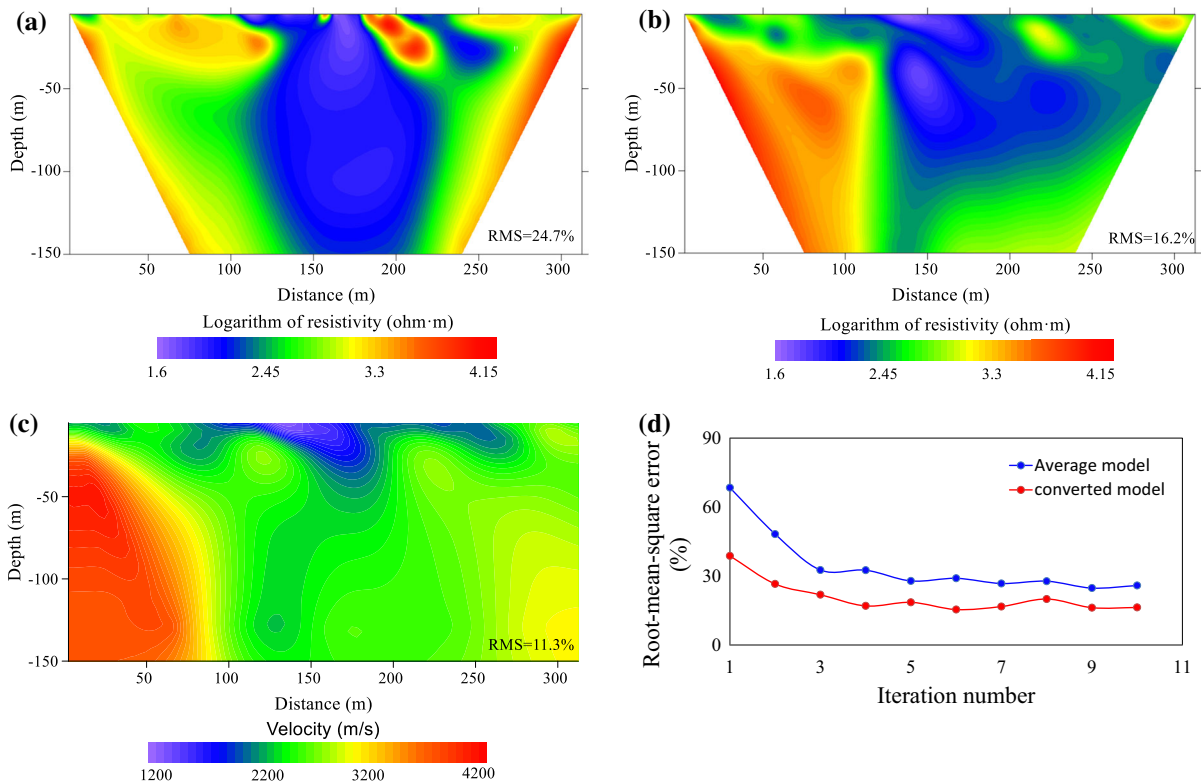
Figure 11
The ERT inversion results from **a** an average prior model; **b** the converted model; **c** the velocity model. **d** RMS errors of ERT inversion from different prior models of Line 1

used in inversion step (Gardner 1939). This step can be easily executed in synthetic models according to their original models. However, for the field data, the original model is not available. Thus, using the simple interpretation of seismic data to return the initial velocity is necessary. Subsequently, we transform the result to the resistivity model, which is used as a prior model for the ERT inversion. The average of the measured apparent resistivity is used as the average prior model for comparison. Figure 11c shows the velocity model with an RMS of 11.3 % after the fifth iteration of Line 1. It is obvious that the survey reveals a subsurface low-velocity area and a high-velocity area in the left portion, where the matching geological properties may indicate a broken-rock zone and entire rock, respectively. Then, these data are converted to a resistivity model for the prior model of the ERT inversion. However, the inversion results from the two

different prior models show different thicknesses for the low-resistivity region (Fig. 11a, b). The RMS level (Fig. 11d) illustrates that the results from the converted prior model better reconstruct the data with an RMS of 16.2 % than the average prior model with an RMS of 24.7 after the tenth iteration. Meanwhile, similar to synthetic data, the RMS error decreases by almost 50 % when the converted prior model is used. Therefore, the converted prior model greatly improves the quality of the electrical resistivity image of Line 1. In particular, the detailed information can help determine water movement, which may be a critical issue impacting the choice of the radioactive waste disposal site.

For Line 2, the velocity model (Fig. 12c) shows a large area of a relatively high-velocity region, which indicates that the measured profile is surrounded entirely by rock in the subsurface area. However, the low-velocity region present in the left corner of the
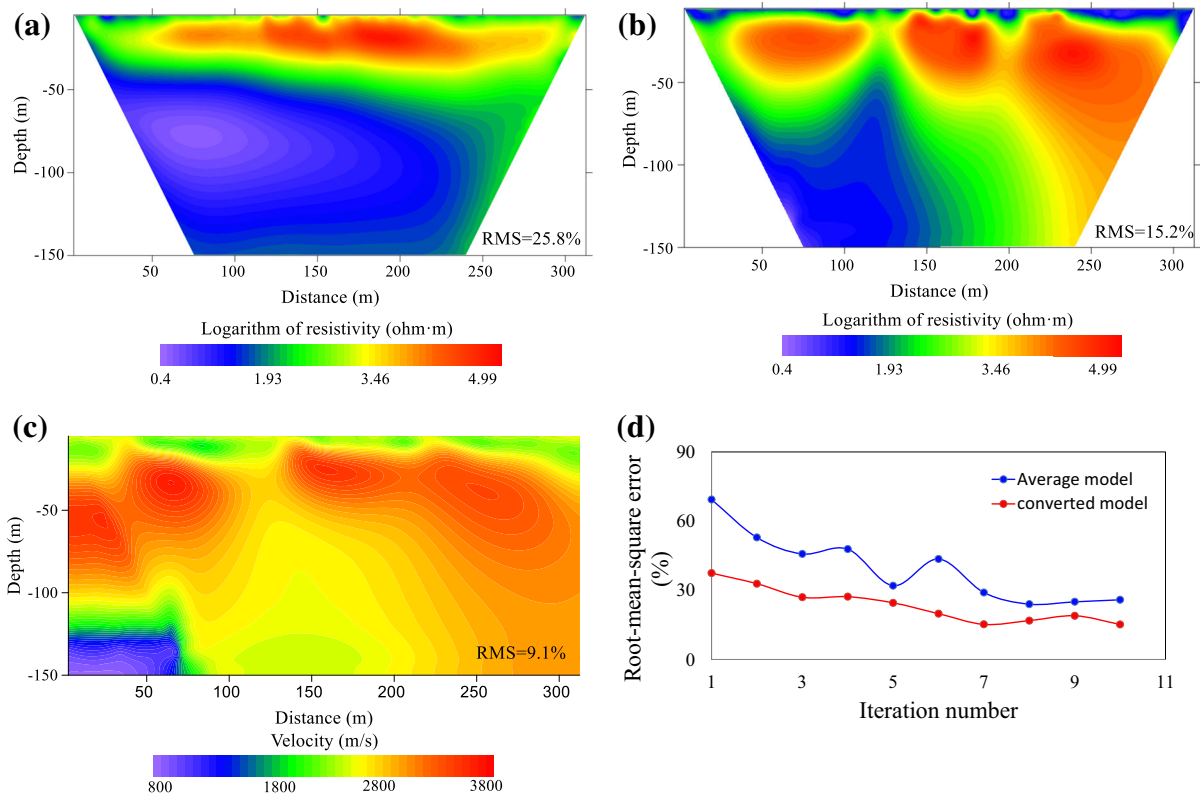
(a)

(b)

(c)

(d)

Figure 12
The ERT inversion results from **a** an average prior model; **b** the converted model; **c** the velocity model. **d** RMS errors of ERT inversion from different prior models of Line 2

profile may be the aquifer, according to local geological data. The resistivity results (Fig. 12a, b) show properties similar to the velocity model. The results from two different prior models reveal that there is a high-resistivity region in the subsurface area of the profile. However, the results from the converted prior model produce more accurate thickness from the high-resistivity data in terms of a lower RMS level. As shown in Fig. 12d, the converted prior model results in the inversion converging more rapidly. Moreover, the lower RMS level in all the iterative calculations greatly reduces the amount of time consumed and the memory requirements associated with computing.

5. Conclusion and Discussion

A new strategy for the reconstruction of resistivity data using inversed seismic data as a prior model has been presented in this work. This work represents an improvement to existing techniques and combines electrical resistivity tomography (ERT) data with seismic data. The ERT inversion algorithm is updated using a patching method that is proven to accelerate the calculations greatly, as compared with RES2Dinv. This strategy is applied to synthetic data and field data. The converted prior model results in a decreased runtime and more accurate results compared with the average prior model. Since the non-unique value of the inversion problem is highly underdetermined, the prior information from seismic data provides the better fit than conventional information to obtain stable solutions for otherwise unstable problems, which has been proved by our synthetic and real example. For the one-block model, the stabilized RMS difference is not obvious between the two initial models. However, the better position and size information of the anomaly was obtained from the converted prior model reconstruction scheme. For the

two-block model, the root-mean-square (RMS) level substantially drops when the converted prior model is used after the first iteration, which reveals the advantage of the strategy in the reconstruction of complicated subsurface structures. From the results of the synthetic models, we conclude that the new strategy is reliable and reasonable and provides a better understanding and characterization of the subsurface structures. The application of the multi-geophysical approach proved to be very useful in the interpretation of field data from the Beishan region. The average prior model exhibits differences in the thicknesses of the geologic layers, whereas the converted model provides a more reasonable geologic scenario according to the RMS level. However, more independent data are still needed to verify that our method presents more accurately subsurface structure. Additionally, we only discuss the 2-D reconstruction technique in this paper. Further development can be achieved by incorporating 3-D ERT and seismic data, which will be studied in future work.

Acknowledgments

REFERENCES

Balia, R., Gavaudo, E., Ardau, F., & Ghiglieri, G. (2003). Geophysical approach to the environmental study of a coastal plain. *Geophysics, 68*, 1446–1459.

Bauman, P. (2005). 2-D resistivity surveying for hydrocarbons—a primer. *CSEG Recorder, 30*, 25–33.

Beauvais, A., Ritz, M., Parisot, J. C., Bantsimba, C., & Dukhan, M. (2004). Combined ERT and GPR methods for investigating two-stepped lateritic weathering systems. *Geoderma, 119*, 121–132.

Cardarelli, E., Cercato, M., Cerreto, A., & Di Filippo, G. (2010). Electrical resistivity and seismic refraction tomography to detect buried cavities. *Geophysical Prospecting, 58*, 685–695.

Chambers, J. C., Kuras, O., Meldrum, P. I., Ogilvy, R. D., & Hollands, J. (2006). Electrical resistivity tomography applied to geologic, hydrogeologic, and engineering investigations at a former waste-disposal site. *Geophysics, 71*, 231–239.

Coppens, F. (1985). First arrival picking on common-offset trace collections for automatic estimation of static corrections. *Geophysical Prospecting, 33*, 1212–1231.

Dahlin, T., Bernstone, C., & Loke, M. H. (2002). A 3-D resistivity investigation of a contaminated site at Lernacken, Sweden. *Geophysics, 67*, 1692–1700.

Gallardo, L. A., & Meju, M. A. (2004). Joint two-dimensional DC resistivity and seismic travel time inversion with cross-gradients constraints. *Journal of Geophysical Research, 109*, B03209.

Gardner, L. W. (1939). An areal plan of mapping subsurface structure by refraction shooting. *Geophysics, 4*, 247–259.

Haeni, F. P. (1986). Application of seismic refraction methods in groundwater modeling studies in New England. *Geophysics, 51*, 236–249.

Hamdan, H. A., & Vafidis, A. (2013). Joint inversion of 2D resistivity and seismic travel time data to image saltwater intrusion over karstic areas. *Environmental Earth Sciences, 68*, 1877–1885.

Hole, J. A. (1992). Nonlinear high-resolution three-dimensional seismic travel time tomography. *Journal of Geophysical Research, 97*, 6553–6562.

Hole, J. A., & Zelt, B. C. (1995). 3-D finite-difference reflection traveltimes. *Geophysical Journal International, 121*, 427–434.

Jarvis, K. D., & Knight, R. J. (2002). Aquifer heterogeneity from SH-wave seismic impedance inversion. *Geophysics, 67*, 1548–1557.

Legault, J. M., Carriere, D., & Petrie, L. (2008). Synthetic model testing and distributed acquisition dc resistivity results over an unconformity uranium target from the Athabasca Basin, northern Saskatchewan. *The Leading Edge, 27*, 46–51.

Leucci, G., Greco, F., De Giorgi, L., & Mauceri, R. (2007). Three-dimensional image of seismic refraction tomography and electrical resistivity tomography survey in the castle of Occhiola (Sicily, Italy). *Journal of Archaeological Science, 34*, 233–242.

Lu, D. B., Zhou, Q. Y., Junejo, S. A., & Xiao, A. L. (2014). A systematic study of topography effect of ERT based on 3-D modeling and inversion. *Pure and Applied Geophysics, 172*, 1531–1546.

Meju, M. A., Gallardo, L. A., & Mohamed, A. K. (2003). Evidence for correlation of electrical resistivity and seismic velocity in heterogeneous near-surface materials. *Geophysical Research Letters, 2003*(30), 7.

Mela, K., & Louie, J. N. (2001). Correlation length and fractal dimension interpretation from seismic data using variograms and power spectra. *Geophysics, 66*, 1372–1378.

Page, L. M. (1968). Use of the electrical resistivity method for investigating geologic and hydrogeologic conditions in Santa Clara County, CA. *Ground Water, 6*, 31–40.

Sumanovac, F., & Weisser, M. (2001). Evaluation of resistivity and seismic methods for hydrogeological mapping in karst terrains. *Journal of Applied Geophysics, 47*, 13–28.

Tarantola, A. (1987). *Inverse problems theory: methods for data fitting and model parameter estimation*. Siam: Elsevier.

Tarantola, A., & Valette, B. (1982). Generalized nonlinear inverse problems solved using the least squares criterion. *Reviews of Geophysics, 20*, 219–232.

Vidale, J. (1988). Finite-difference calculation of travel times. *Bulletin of the Seismological Society of America, 78*, 2062–2076.

White, R. M. S., Collins, S., Denne, R., Hee, R., & Brown, P. (2001). A new survey design for 3D IP modelling at Copper Hill. *Exploration Geophysics, 32*, 152–155.

Wilson, S. R., Ingham, M., & McConchie, J. A. (2006). The applicability of earth resistivity methods for saline interface definition. *Journal of Hydrology, 316*, 301–312.

Zelt, C. A., & Barton, P. J. (1998). Three-dimensional seismic refraction tomography: a comparison of two methods applied to data from the Faeroe Basin. *Journal of Geophysical Research: Solid Earth, 103*, 7187–7210.